Measurement and microscopic analysis of the $^{11}B(\vec{p},\vec{p})$ reaction at $E_p = 150$ MeV. II. Depolarization in elastic scattering from odd-*A* nuclei

V. M. Hannen,[1,*] K. Amos,[2] A. M. van den Berg,[1] R. K. Bieber,[1,†] P. K. Deb,[2] F. Ellinghaus,[3,‡] D. Frekers,[3] M. Hagemann,[4] M. N. Harakeh,[1] J. Heyse,[4,§] M. A. de Huu,[1] B. A. M. Krüsemann,[1,‖] S. Rakers,[3] R. Schmidt,[3] S. Y. van der Werf,[1] and H. J. Wörtche[1]

[1]*Kernfysisch Versneller Instituut, Zernikelaan 25, NL-9747 AA Groningen, The Netherlands*

[2]*School of Physics, University of Melbourne, Victoria 3010, Australia*

[3]*Institut für Kernphysik, Westfälische Wilhelms Universität, D-48149 Münster, Germany*

[4]*Vakgroep Subatomaire en Stralingsfysica, Universiteit Gent, B-9000 Gent, Belgium*

(Received 27 November 2002; published 30 May 2003)

The polarization-transfer coefficient $D_{nn'}$ in the elastic scattering of 150-MeV protons from ^{11}B has been measured in the angular range $5° < \theta_{\text{c.m.}} < 31°$. Significant deviations of $D_{nn'}$ from unity are observed starting around a center-of-mass scattering angle of 23°. The observed angular variation of $D_{nn'}$ is analyzed using phenomenological and microscopically generated optical-model potentials to describe the monopole attributes of elastic scattering and to generate the distorted waves used in a distorted-wave approximation evaluation of nonzero multipole contributions to the elastic scattering process. The same approach is used to analyze datasets of $D_{nn'}$ in elastic scattering from ^{13}C and off ^{15}N, which are available in the literature. The agreement of the fully microscopic analysis with the data is comparable or, in the case of ^{11}B, slightly better than what is achieved with conventional phenomenological optical-model calculations.

DOI: 10.1103/PhysRevC.67.054321 PACS number(s): 25.40.Cm, 27.20.+n, 24.70.+s

I. INTRODUCTION

The description of elastic scattering of protons from a target nucleus conventionally uses a phenomenological optical potential [1]. This potential contains a number of free parameters that are adjusted to deliver a good fit to measured data. Microscopic models of elastic scattering, where an optical potential is derived by folding the ground-state density of the target nucleus with an effective nucleon-nucleon (*NN*) interaction, have been reviewed recently [2] and are predictive in that all facets involved in the calculation of scattering observables are preset. There are no *a posteriori* adjustments allowed in the most stringent application. The latter approach avoids ambiguities that come about in the determination of the free parameters of the phenomenological optical potential [1], but requires sophisticated models of the effective *NN* interaction and a realistic description of the ground state of the target nucleus to give accurate results for the observables of the scattering process [3]. In Ref. [2] methods are discussed to define an effective interaction (in coordinate space) and to perform the folding yielding a nonlocal optical potential. In this approach, exchange knockout scattering is allowed since antisymmetrization of the projectile and target nucleon wave-function product is treated explicitly. Those methods are implemented in the distorted-wave code DWBA98 [4].

A way to include medium effects in the description of nucleon-nucleus scattering is provided by the *NN g* matrices: solutions of the (infinite matter) Brückner-Bethe-Goldstone equations with the local density within a nucleus related as usual to the value of the Fermi momentum. Various sets of *g* matrices have been developed based upon different starting forms of the free *NN* interaction. To form an effective *NN* interaction in coordinate space that can be used in scattering programs such as DWBA98, a mapping of those *g* matrices needs to be made. The effective interaction (for use in DWBA98) has central, spin-orbit, and tensor terms, each with a form factor that is a combination of Yukawa functions. The medium influence defining the *g* matrices reflects in the strengths of those Yukawa functions being complex and energy and density dependent. Starting with the Paris interaction [5], Von Geramb [6] developed one of the first ''realistic'' effective *NN* interactions. Later, Nakayama and Love [7] as well as the Melbourne group [2,8] have used various Bonn interactions [9] as a starting point. As mentioned in the previous paper [10], use of the medium-modified interaction developed by the Melbourne group results in close reproductions of the elastic scattering data obtained by scattering 150-MeV protons from ^{11}B and ^{12}C nuclei.

Note that both phenomenological optical potentials and potentials following from a folding procedure describe only the monopole part of the elastic scattering process. Target nuclei with a nonzero ground-state spin, such as ^{11}B with $J^\pi = 3/2^-$, allow for higher-order multipole contributions to the elastic scattering. These higher-order contributions contain spin-flip parts that cause the polarization-transfer coefficient $D_{nn'}$ to deviate from unity. Measurements of depolarization effects in elastic scattering have, among others, been performed by Von Przewoski *et al.* [11] and Nakano *et al.* [12,13]. These data have up to now been interpreted either in

*Present address: SRON, Sorbonnelaan 2, 3584 CA Utrecht, The Netherlands. Electronic address: v.m.hannen@sron.nl

†Present address: Universität Köln, Germany.

‡Present address: DESY Zeuthen, Germany.

§Present address: EC, JRC, IRMM, Geel, Belgium.

‖Present address: ASF Thomas Industries GmbH & Co.KG, Wuppertal, Germany.

a completely phenomenological way, by adding spin-spin terms to the base optical-model potential which are then adjusted to reproduce the observations, or in a semimicroscopic approach, where the $\Delta J=0$ contribution to the transition is described by a phenomenological optical potential and the higher-multipole contributions follow from a microscopic distorted wave Born approximation (DWBA) analysis using nuclear structure input obtained from shell-model calculations.

In the present work we will describe the measurement of the polarization-transfer coefficient $D_{nn'}$ for the elastic scattering of 150-MeV polarized protons from ^{11}B. Results obtained for the ^{11}B case were cross-checked by elastic-scattering measurements using a ^{12}C target, where $D_{nn'}$ is equal to unity. It should be emphasized that both elastic and inelastic scattering data for a particular target in this experiment (either ^{11}B or ^{12}C) were obtained using the same settings of the whole system, i.e., ion source, accelerator, beam tune, spectrometer, and detector system. Only the targets (alternating the ^{11}B and ^{12}C targets), spin states (up, down, or off), and the spectrometer angles (and thus the magnetic field settings of the spectrometer) were changed during the experiment.

The results obtained for the excitation of states in ^{11}B as well as most of the experimental details have been presented in the previous paper [10]. Thus, we describe in Sec. III only those experimental details that are specific to the work contained herein. In Sec. IV measurements of polarization observables in elastic scattering from ^{11}B and ^{12}C are displayed. One example is given of polarization observables obtained for the inelastic transition to the $J^{\pi}=3/2^{-}$ state at $E_x=5.020$ MeV. For the other strong inelastic transitions, however, polarization-transfer coefficients have been discussed in Ref. [10] and will only be touched upon briefly. Then in Sec. V elastic scattering data obtained for ^{11}B in this experiment and data for elastic scattering from ^{13}C ^{15}N, which are available in the literature [11,13,12], are compared to the results of both semimicroscopic and fully microscopic model calculations. Finally, in Sec. VI, we summarize our findings. First, however, the concept of polarization observables is introduced.

II. POLARIZATION PARAMETERS

The general treatment for the relations between polarization-transfer coefficients is described in detail by Ohlsen [14]; the specific case for the present setup is given in Ref. [15]. Here, we only show the basic formulas relevant for this analysis. As explained in Ref. [14], polarization-transfer experiments are usually described in so-called helicity frames. These are systems moving along with the particle, whose basis vectors $\hat{s}$, $\hat{n}$, and $\hat{l}$ (for sideways, normal, and longitudinal) are given by the in- and outgoing momenta $\vec{k}_{in}$ and $\vec{k}_{out}$ of the projectile and ejectile. The incoming helicity frame is defined by

$$\hat{n}=\frac{\vec{k}_{in}\times\vec{k}_{out}}{|\vec{k}_{in}\times\vec{k}_{out}|},$$

$$\hat{l}=\frac{\vec{k}_{in}}{|\vec{k}_{in}|},$$

$$\hat{s}=\hat{n}\times\hat{l}, \tag{1}$$

and the basis vectors of the outgoing helicity frame $\hat{s}'$, $\hat{n}'$, and $\hat{l}'$ are defined accordingly with

$$\hat{n}'=\hat{n},$$

$$\hat{l}'=\frac{\vec{k}_{out}}{|\vec{k}_{out}|},$$

$$\hat{s}'=\hat{n}'\times\hat{l}'. \tag{2}$$

The polarization vectors before and after the scattering are labeled $\vec{p}$ and $\vec{p}'$, respectively. The differential cross section $I(\theta,\phi)$ for a polarized beam is given by

$$I(\theta,\phi)=I_0(\theta)\left(1+\sum_{i=1}^{3} p_i A_i(\theta)\right), \tag{3}$$

where $I_0(\theta)$ is the cross section for an unpolarized beam and $A_i(\theta)$ is the analyzing power for the ith component of the incoming polarization p_i. The components of the outgoing polarization $p'_{j'}$ are given by

$$p'_{j'}I(\theta,\phi)=I_0(\theta)\left(P_{j'}(\theta)+\sum_{i=1}^{3} p_i D_{ij'}(\theta)\right), \tag{4}$$

where $P_{j'}$ is the j'th component of the induced polarization which would be obtained by the scattering of an unpolarized beam, and $D_{ij'}$ is the polarization-transfer coefficient connecting the ith component with the j'th component of the incoming and outgoing polarization vectors, respectively.

From Eqs. (3) and (4) it seems that there are, in total, 15 polarization observables (three analyzing powers A_i, three induced polarizations $P_{j'}$, and a 3×3 matrix of polarization-transfer coefficients $D_{ij'}$). Some of them, however, are zero because of parity conservation.

$$\begin{aligned} A_s=A_l=0,\\ P_{s'}=P_{l'}=0,\\ D_{sn'}=D_{ns'}=D_{nl'}=D_{ln'}=0, \end{aligned} \tag{5}$$

reducing Eqs. (3) and (4) to

$$I(\theta,\phi)=I_0(\theta)[1+p_n A_n(\theta)] \tag{6}$$

and

$$\begin{pmatrix} p'_{s'} \\ p'_{n'} \\ p'_{l'} \end{pmatrix} I(\theta,\phi) = I_0(\theta)\left[\begin{pmatrix} 0 \\ P_{n'} \\ 0 \end{pmatrix} + \begin{pmatrix} D_{ss'} & 0 & D_{ls'} \\ 0 & D_{nn'} & 0 \\ D_{sl'} & 0 & D_{ll'} \end{pmatrix} \times \begin{pmatrix} p_s \\ p_n \\ p_l \end{pmatrix}\right]. \quad (7)$$

As elastic scattering is invariant under time reversal, it can be shown that one has the following equalities:

$$A_n = P_{n'}, \quad D_{sl'} = -D_{ls'}. \quad (8)$$

A frequently used quantity for polarization-transfer experiments is the transverse spin-flip probability $S_{nn'}$ which is defined by

$$S_{nn'} = \frac{1}{2}(1 - D_{nn'}). \quad (9)$$

Once the beam polarization and the outgoing polarization, produced in a particular nuclear reaction, have been established, it is possible to extract some of the polarization observables contained in Eq. (7). A complication arises because polarization observables are defined in helicity coordinates while incoming and outgoing polarizations are measured in laboratory systems fixed by the experimental setup. Some extra steps are therefore required to derive the dependence of the measured polarizations on the polarization observables in the laboratory system. In the present experiment, the incoming polarization vector was aligned with the vertical direction in the laboratory coordinate system: $\vec{p} = (0, p_y, 0)$. At spectrometer angles $\theta \geqslant 10°$ one can then derive the following approximation [15]:

$$\overline{p'_y}\left(1 + p_y A_n(\theta)\frac{1}{N}\sum_{ev.}\cos\phi\right) \approx D_{nn'} p_y \frac{1}{N}\sum_{ev.}\cos^2\phi + P_{n'}\frac{1}{N}\sum_{ev.}\cos\phi, \quad (10)$$

where $\overline{p'_y}$ is the outgoing polarization averaged over all azimuthal angles ϕ that fall into the acceptance of the BBS and the sums run over all events N. Equation (10) allows an extraction of $D_{nn'}$ and $P_{n'}$ from any two measurements with different incoming polarizations.

III. EXPERIMENTAL PROCEDURE AND DATA REDUCTION

As described in the earlier paper [10], the data were obtained during a running period of 5 days using the AGOR facility of the KVI. To obtain a polarized proton beam, the atomic-beam source POLIS [16] was used. Elastically (and inelastically) scattered protons were momentum analyzed with the Big-Bite Spectrometer (BBS) [17] and detected in the EUROSUPERNOVA detection system, which consists of a focal-plane detection system and a focal-plane polarimeter (FPP), both described in Ref. [18]. The analysis of the elastic data presented in this paper was performed in exactly the same way as the treatment of the inelastic data discussed in the previous paper [10].

To be able to measure vector as well as tensor polarizations, the in-beam polarimeter (IBP) [19] of the KVI is made up of 16 detectors grouped into four planes at $-45°$, $0°$, $45°$, and $90°$ around a CH_2 or CD_2 target. The four detectors of a plane are set up as pairs matching certain kinematic conditions to measure the ejectile and the recoil particle of either proton-proton or proton-deuteron reactions in coincidence. By measuring differences in the coincidence rates of particles scattered to the left and to the right in the detector planes it is possible to deduce the polarization of the incoming beam if the analyzing power of the reaction is known. Instrumental asymmetries are determined by measurements with an unpolarized beam and are corrected for in the calculation of the beam polarizations. In order to provide a ''completely'' unpolarized beam, not only the transition units of the atomic-beam ion source, but also the hexapole magnet that focuses the beam inside the source, have been switched off, and data obtained under these conditions will be referred to as ''hexapole-off'' measurements. In this experiment, the IBP was set up to detect proton-proton coincidences. The analyzing power for proton-proton scattering can be obtained from the *NN*-online facility of the University of Nijmegen [20] which performs calculations based on nucleon-nucleon potentials described in Ref. [21]. Pairs of coincident detectors were placed at $19.0°$ and $69.6°$ scattering angles (corresponding to a center-of-mass angle of $39.7°$) selecting the maximum value $A_n = 0.222$ of the analyzing power for 150-MeV protons.

To reduce errors in the measurement of the polarization of the beam by changes in the beam profile at the IBP target position, a spot target was used consisting of a 100 mg/cm^2 CH_2 foil with a diameter of 2 mm placed on a 4-μm-thin aluminum backing. Unfortunately, the target had a substantial impact on the beam quality, leading to background problems in the BBS detectors. We therefore decided to measure the beam polarization in regular intervals in between the BBS measurements and not to use the IBP and the BBS simultaneously.

Figure 1 shows the measured normal and sideways components of the beam polarization for the three modes of operation of the transition units of POLIS; these modes are: strong field transition on, weak field transition on, and both transition units switched off. The beam polarization obtained in the spin-off mode of POLIS (in which only the transition units are switched off) has a nonzero value. This is consistent with findings with a similar source at Saturne [22] and is the reason to perform ''hexapole-off'' measurements instead of using the spin-off data as reference for the calculation of the other spin states.

The changes in the measured polarization over time cannot be attributed only to the ion source because this would not explain rises of as much as 5% above the mean value. Instead, the observed fluctuations must be due to a combina-

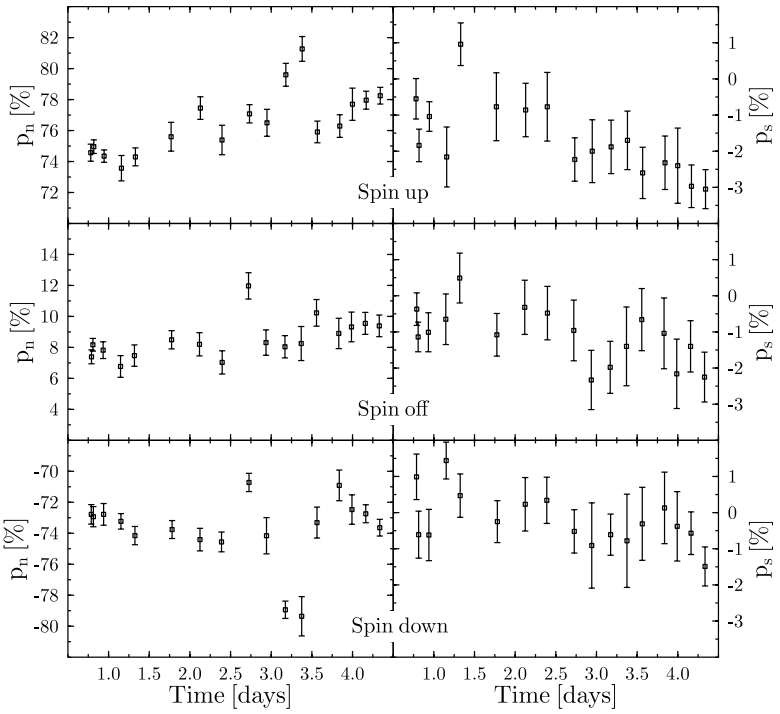

FIG. 1. Normal and sideways components of the 150-MeV proton beam measured over the five-day period of the experiment using the IBP.

tion of real polarization changes and effects caused by components located upstream of the IBP. At this time it is not clear which components have added to these fluctuations. For the present analysis it is assumed that there is one value for the polarization of each spin state and the fluctuations seen in the data are taken into account by increasing the error bar on the data points so that the χ^2 value of the mean is taken to be 1. The resulting polarization values and total errors for the three spin states are listed in Table I. The sideways component of the beam polarization, though not consistent with zero for the spin-up and spin-off states, is very small and will be neglected in the analysis.

The method applied to determine proton polarizations in the FPP is the measurement of an asymmetry in the azimuthal distribution of a secondary scattering of the protons in a graphite analyzer. This requires that the particle tracks before and after the analyzer are reconstructed on an event-per-event basis. From the resulting angular distribution one can calculate the transverse components of the outgoing polarization using an estimator formalism [23], provided that the inclusive proton-carbon analyzing power $A_c(\theta_c)$, at the particular proton energy and particular secondary-scattering angle θ_c, is known.

TABLE I. Polarization values and uncertainties of the three spin states produced by POLIS during the experiment.

Spin up	p_n	76.2	$\pm 1.6\%$
	p_s	-1.6	$\pm 0.6\%$
Spin off	p_n	8.3	$\pm 0.8\%$
	p_s	-1.0	$\pm 0.3\%$
Spin down	p_n	-73.7	$\pm 1.7\%$
	p_s	-0.1	$\pm 0.4\%$

Because the polarization is calculated from an asymmetry measurement, care has to be taken to correct for possible instrumental asymmetries inherent to the detector setup. The results of this analysis and the determination of the inclusive proton-carbon scattering analyzing power $A_c(\theta_c)$ will be described elsewhere [15]. A number of software cuts were set on the data obtained from the polarimeter. These were a cut on the cone for scattering of the protons in the graphite analyzer ($5° < \theta_c < 25°$) and a cut on the solid-angle acceptance of the spectrometer (the bin size for the polar scattering angle θ was limited to 1.5°, the azimuthal scattering angle ϕ was limited to $|\phi| \leqslant 15°$). For inelastic transitions, however, the limit on the polar angle acceptance was released, but the cut on the azimuthal angle was maintained. In addition, for all data, limits were set on the vertex reconstruction for the scattering of the protons in the graphite analyzer; these last cuts reject in total about 16% of the acquired data for secondary scattering angles larger than 4° [15].

Because there can be a smooth variation in the cross sections and analyzing powers over the area covered by the BBS acceptance, average values

$$\overline{\theta} = \frac{1}{N} \sum_{ev.} \theta, \qquad \overline{A_n} = \frac{1}{N} \sum_{ev.} A_n(\theta), \tag{11}$$

have been used for the scattering angle and the analyzing power of the reaction at a particular spectrometer angle.

IV. RESULTS

Figure 2 shows the resulting distributions of $D_{nn'}$ and $P_{n'} - A_n$ for elastic scattering from ^{12}C and ^{11}B and an ex-

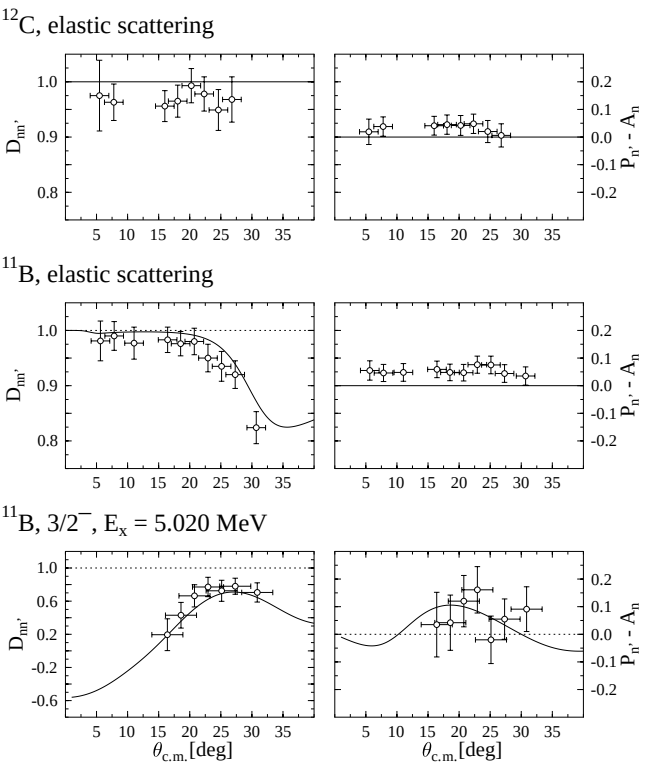

FIG. 2. Measured distributions of $D_{nn'}$ and $P_{n'}-A_n$ for elastic scattering of 150-MeV protons from ^{12}C (upper panel), ^{11}B (middle panel), and for the inelastic transition to the $3/2^-$ state at 5.020 MeV in ^{11}B (lower panel). Solid lines indicate the results of microscopic DWBA calculations, which are discussed in Sec. V for elastic scattering and in Ref. [10] for inelastic scattering.

ample of the angular distribution obtained for one of the inelastic transitions in ^{11}B. Elastic-scattering data provide a test of the validity of the analysis procedure through the relations $P_{n'}-A_n=0$ and $D_{nn'}=1$ (and therefore $S_{nn'}=0$). The latter is only fulfilled for the elastic scattering from nuclei with a zero ground-state spin and in the case of nuclei with a nonzero ground-state spin at small scattering angles, where higher multipolarities in the reaction mechanism can be neglected. The measured distributions for elastic scattering exhibit small offsets from these values, which are observed consistently for both ^{12}C and ^{11}B (see Table II).

There are several sources of systematic uncertainties, which might cause these offsets. Systematic errors in the beam polarizations have an important impact because the incoming polarization p_n enters twice in the calculation of the polarization observables. This occurs directly via Eq. (10) and indirectly via the analyzing power of the reaction, which is calculated from measured cross sections and beam polarizations. Other possible causes for systematic uncertainties are the parametrization of the effective proton-carbon analyzing power and remaining instrumental asymmetries of the FPP. As the observed offsets are small (in case of the spin-flip probability $S_{nn'}$ they are between 0.01 and 0.02) and can be subtracted from the angular distributions of the polarization observables, they pose no problem for the interpretation of the data.

TABLE II. Deviation from unity for the polarization observable $D_{nn'}$ and offsets for the polarization observables $S_{nn'}$ and $P_{n'}-A_n$ observed in the elastic scattering data from ^{12}C and ^{11}B.

	^{12}C	^{11}B	^{11}B ($\theta<20°$)
$1-D_{nn'}$	0.03 ± 0.01		0.02 ± 0.01
$S_{nn'}$	0.016 ± 0.006		0.010 ± 0.005
$P_{n'}-A_n$	0.035 ± 0.009	0.050 ± 0.007	

V. COMPARISON WITH CALCULATIONS

A. Elastic scattering from ^{11}B

Data were analyzed both in a semimicroscopic and in a fully microscopic approach, where the monopole part of the elastic scattering follows from a folding of the medium-modified effective *NN* interaction given by the Melbourne group with the ground-state density of the target nucleus, which has been calculated using the OXBASH shell-model code [24]. The ground-state density is specified in terms of occupation numbers of the single-particle states calculated in a $0\hbar\omega$ model space. The resulting average number of particles in each orbit is for ^{11}B: $1s_{1/2}=2$, $1p_{3/2}=2.650$ and $1p_{1/2}=0.350$ for protons and $1s_{1/2}=2$, $1p_{3/2}=3.274$ and $1p_{1/2}=0.726$ for neutrons. Occupation numbers obtained in a complete $(0+2)\hbar\omega$ model space have also been tested, but did not produce a significant difference in the optical-potential results. One-body transition densities, which are necessary to calculate the higher-order multipole contributions to the elastic scattering process were calculated in a complete $(0+2)\hbar\omega$ model space using the MK3W interaction which is part of the OXBASH code package (for more details on the shell-model calculations, see Ref. [10]). The same one-body transition densities were used in the semimicroscopic and in the fully microscopic calculations.

In Fig. 3, the results of semimicroscopic calculations of the cross section, analyzing power, and polarization-transfer coefficient $D_{nn'}$ of the elastic scattering of 150-MeV protons from ^{11}B are compared with data from the present experiment and with data from an earlier measurement performed by Geoffrion *et al.* [25]. Those semimicroscopic calculations required optical-potential parameters that have been obtained from Ref. [26]. Although this parameter set was originally intended for elastic proton scattering from ^{12}C, it results in a much better fit to the measurements than parameters that have been derived for the ^{11}B case at the appropriate proton energy [25]. Given that this potential was chosen to fit data from the nearby nucleus ^{12}C, it is no surprise that the calculated cross section and analyzing power (for $\theta_{c.m.}\leqslant30°$) describe our data for the scattering from ^{11}B well. Note that the experimental data on $D_{nn'}$ have been corrected for the offset given in Table II.

The results of our fully microscopic analysis are presented in Fig. 4. It should be stressed that in this case the results are predictions. There is a very good agreement between the calculated and measured differential cross sections. The predicted analyzing power correctly describes the angular variation of the data while the magnitudes of the maxima cannot

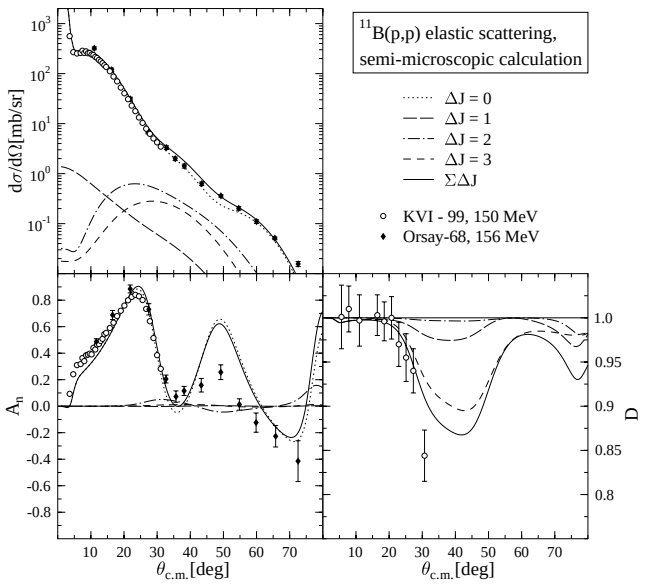

FIG. 3. Semimicroscopic calculation of the ^{11}B(p,p) elastic-scattering cross section, analyzing power, and polarization-transfer coefficient $D_{nn'}$ applying a set of optical-model parameters obtained from Ref. [26]. The data from the present analysis are shown as the open circles; for the $D_{nn'}$ values corrections have been made for the deviation from unity as listed in Table II. The ''Orsay-68'' dataset is taken from Ref. [25].

be reproduced. We note that the overestimation of the second maximum is also observed in the semimicroscopic calculation. The angular distribution of the polarization-transfer coefficient $D_{nn'}$ is correctly reproduced over the complete measured region.

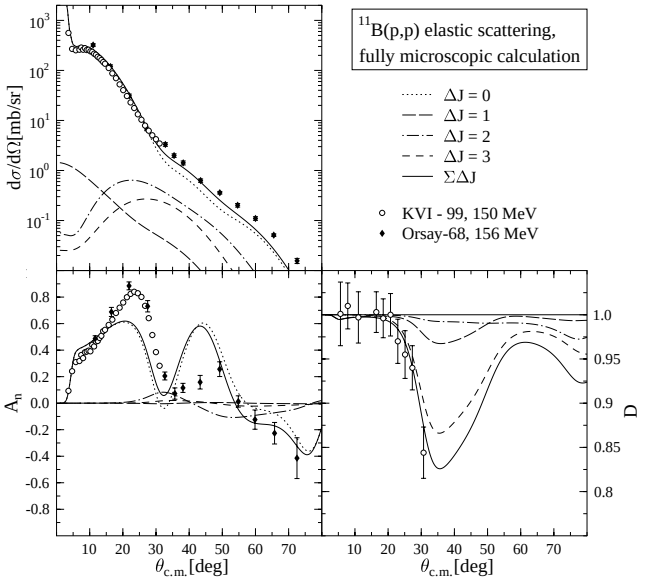

FIG. 4. Fully microscopic calculation of the ^{11}B(p,p) elastic-scattering cross section, analyzing power, and polarization-transfer coefficient $D_{nn'}$. The data from the present analysis are shown as the open circles; for the $D_{nn'}$ values corrections have been for the deviation from unity as listed in Table II. The ''Orsay-68'' dataset is taken from Ref. [25].

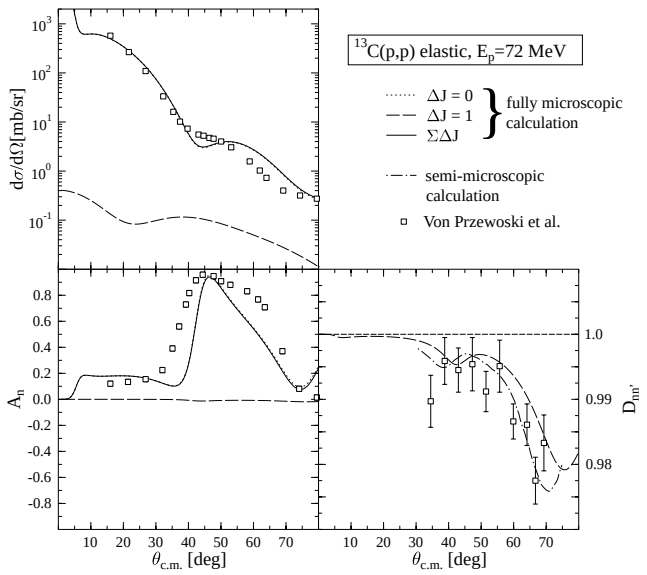

FIG. 5. Elastic scattering of 72-MeV protons from ^{13}C. Angular distributions of the $\Delta J=0$ transfer and of the sum of J transfers are nearly overlapping in the cross section and analyzing power plots. The experimental data and the semimicroscopic calculation of the polarization-transfer coefficient $D_{nn'}$ are taken from Ref. [11].

Both types of calculations predict that the largest contribution to the observed depolarization effect stems from the octupole part $(\Delta J=3)$ of the transition. It is unfortunate that no data points are available at larger scattering angles to fix the position of the maximum of the distribution. For the ^{11}B case, it can be concluded that the fully microscopic approach gives a good description of the observables of the elastic scattering process.

B. Elastic scattering from ^{13}C and ^{15}N

To verify the conclusions of the preceding section, two more cases known from the literature have been studied, namely, ^{13}C and ^{15}N. Both nuclei have a ground-state spin $J^{\pi}=1/2^{-}$. In these cases only the dipole $(\Delta J=1)$ part of the transition can change the spin orientation of the projectile and the observable depolarization effects are therefore expected to be smaller.

The elastic ^{13}C$(\vec{p},\vec{p})$ reaction has been measured by Von Przewoski *et al.* at an incoming proton energy of 72 MeV [11]. Data obtained in this experiment are shown together with the results of a fully microscopic analysis (indicated by solid and dashed lines) in Fig. 5. The result of a semimicroscopic analysis of the depolarization effect [11] is indicated by the dash-dotted line in the lower right plot of the figure. Except for a small shift in the calculated angular distributions of about 5°, which might be due to the use of a different harmonic oscillator parameter, the two approaches give similar results.

The ^{15}N case has been studied by Nakano *et al.* [13,12] at an incoming proton energy of 65 MeV and angular distributions of the analyzing power, and the polarization-transfer coefficient $D_{nn'}$ have been published. Semimicroscopic calculations of the depolarization have been performed by Von

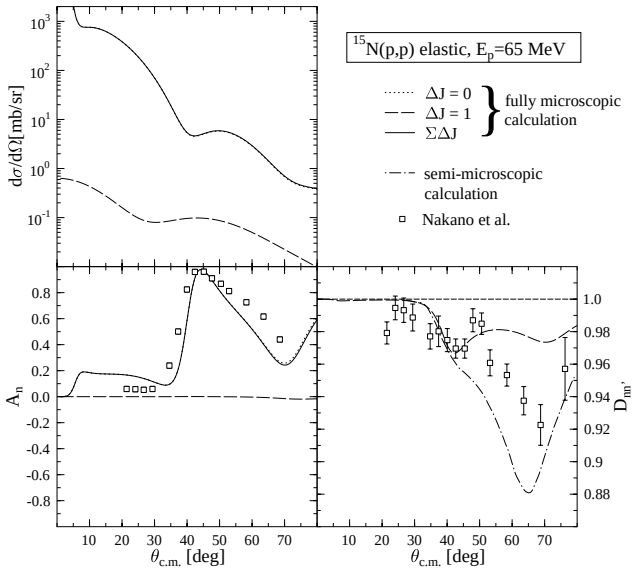

FIG. 6. Elastic scattering of 65-MeV protons from ^{15}N. Angular distributions of the $\Delta J=0$ transfer and of the sum of J transfers are nearly overlapping in the cross section and analyzing power plots. The experimental data have been taken from Refs. [13,12] and the semimicroscopic calculation of the polarization-transfer coefficient $D_{nn'}$ is taken from Ref. [11].

Przewoski *et al.* [11] and are compared to the results of a fully microscopic analysis in Fig. 6. The observed effect for ^{15}N is much stronger than for ^{13}C and in contrast to the ^{11}B and ^{13}C cases there are large discrepancies between the experimental data, the result of the fully microscopic calculation, and the result of the semimicroscopic approach. The size of the observed effect is explained by Von Przewoski *et al*. with the special structure of the ^{15}N nucleus, which has a transverse form factor that is about ten times larger than for ^{13}C [27]. The large difference between the fully microscopic and the semimicroscopic calculations at angles $\theta_{\mathrm{c.m.}} \geqslant 40°$ may have several origins. In the semimicroscopic model calculations, the optical-potential parameters used may not have been optimal. Von Przewoski *et al.* note that the optical-model parameters applied in the calculation have been extrapolated from nearby nuclei and were not obtained from a fit to ^{15}N data directly. Variation between the results is also expected due to differences in the nuclear wave functions applied in the two calculations. Finally, there may be shortcomings in the effective nucleon-nucleon interaction at large q transfers.

VI. SUMMARY AND CONCLUSION

The analysis procedures developed in Ref. [15] have been put to test by analyzing elastic proton scattering from ^{12}C, where the extracted spin-flip probability $S_{nn'}$ and the difference between the induced polarization and the analyzing power $|P_{n'}-A_n|$ should be zero. Both measured quantities exhibit a small offset from this prediction. The offset is less than 0.02 for $S_{nn'}$ (allowed range $0 \leqslant S_{nn'} \leqslant 1$) and below 0.025 for $|P_{n'}-A_n|$ (allowed range: $|P_{n'}-A_n| \leqslant 2$). There are several possible sources for the observed offsets. Systematic uncertainties in the measured beam polarizations have an important impact, as the incoming polarization enters twice into the extraction of polarization observables. Other possible systematic uncertainties may arise from shortcomings in the parametrization of the inclusive p-C analyzing power or from remaining instrumental asymmetries that cannot be corrected for by the procedures discussed in Ref. [15].

Two different approaches have been taken to describe elastic scattering from ^{11}B and from two other nuclei with a nonzero ground-state spin, namely, ^{13}C and ^{15}N. The nonzero spin of these nuclei allows for higher-order multipole contributions to the elastic scattering process. These contributions cause the polarization-transfer coefficient $D_{nn'}$ to deviate from unity and are evaluated using a DWBA approach. Conventional, ''semimicroscopic'' calculations, where the distorted waves are generated from a phenomenological optical potential, have been compared with fully microscopic calculations, applying a folding potential to generate distorted waves. As the semimicroscopic calculations by definition give a good description of cross sections and analyzing powers, the comparison is based on the observed depolarization effects in the above mentioned nuclei.

Experimental data and semimicroscopic calculations for ^{13}C and ^{15}N have been taken from Refs. [11,13,12]. For ^{11}B and ^{13}C the fully microscopic analysis gives a similar or, in the case of ^{11}B, slightly better description of $D_{nn'}$ than the semimicroscopic calculations. For ^{15}N neither of the two calculations matches the data, with the fully microscopic calculation underestimating the effect and the semimicroscopic approach overestimating it. The reasons for the observed discrepancies in the ^{15}N case are unclear and might be an interesting subject for additional experimental and theoretical investigations. From the comparison of the two types of calculations it may be concluded that, by using state-of-the-art parametrizations of the effective nucleon-nucleon interaction, one can avoid the use of phenomenological optical potentials and the ambiguities related to the determination of their parameters in the description of proton scattering experiments.

ACKNOWLEDGMENTS

We acknowledge H. Sakai for providing the enriched ^{11}B target and the cyclotron crew of AGOR for their assistance throughout the experiment. This work was performed as part of the research program of the Stichting voor Fundamenteel Onderzoek der Materie (FOM) with financial support from the Nederlandse Organisatie voor Wetenschappelijk Onderzoek (NWO) and the Fund for Scientific Research (FSR) Flanders. It was supported by the European Community through the Human Capital and Mobility Program under Contract No. ERBCHRX-CT94-0562 and the Land Nordrhein-Westfalen. Two of us (K.A. and P.K.D.) gratefully acknowledge the support provided by a research grant from the Australian Research Council.

[1] P. E. Hodgson, *Proceedings of the Specialists' Meeting on the Nucleon Nucleus Optical Model up to 200 MeV* (OECD Nuclear Energy Agency, Paris, 1996).
[2] K. Amos, P.J. Dortmans, H.V. Von Geramb, S. Karataglidis, and J. Raynal, Adv. Nucl. Phys. **25**, 275 (2000).
[3] P.J. Dortmans and K. Amos, Phys. Rev. C **49**, 1309 (1994).
[4] J. Raynal, computer code DWBA98, NEA Data Services, NEA-1209/005 (1998).
[5] M. Lacombe, B. Loiseau, J.M. Richard, R. Vinh Mau, J. Côté, P. Pirès, and R. de Tourreil, Phys. Rev. C **21**, 861 (1980).
[6] H.V. Von Geramb, in *The Interaction Between Medium Energy Nucleons in Nuclei—1982*, edited by H. O. Meyer, AIP Conf. Proc. No. 97 (AIP, New York, 1983), p. 44.
[7] K. Nakayama and W.G. Love, Phys. Rev. C **38**, 51 (1988).
[8] P.K. Deb and K. Amos, Phys. Rev. C **62**, 024605 (2000).
[9] R. Machleidt, K. Holinde, and Ch. Elster, Phys. Rep. **149**, 1 (1987).
[10] V. M. Hannen *et al.*, Phys. Rev. C **67**, 054320 (2003), preceding paper.
[11] B. Von Przewoski *et al.*, Nucl. Phys. **A528**, 159 (1991).
[12] T. Nakano *et al.*, RCNP Annual Report 1987, p. 3 (1987).
[13] T. Nakano *et al.*, Phys. Lett. B **240**, 301 (1990).
[14] G.G. Ohlsen, Rep. Prog. Phys. **35**, 717 (1972).
[15] V. M. Hannen *et al.*, Nucl Instrum. Methods Phys. Res. A **500**, 68 (2003).
[16] H.R. Kremers and A.G. Drentje, in *Polarized Gas Targets and Polarized Beams*, edited by J. Holt and Michael A. Miller, AIP Conf. Proc. No. 421 (AIP, Woodbury, NY, 1997), p. 507.
[17] A.M. van den Berg, Nucl. Instrum. Methods Phys. Res. B **99**, 637 (1995).
[18] H.J. Wörtche, Nucl. Phys. **A687**, 321c (2001).
[19] R. Bieber *et al.*, Nucl. Instrum. Methods Phys. Res. A **457**, 12 (2001).
[20] M. Rentmeester and R. A. M. Klomp, NN-Online, http://nn-online.sci.kun.nl (1994).
[21] V.G.J. Stoks, R.A.M. Klomp, C.P.F. Terheggen, and J.J. de Swart, Phys. Rev. C **49**, 2950 (1994).
[22] C.E. Allgower *et al.*, Nucl. Instrum. Methods Phys. Res. A **399**, 171 (1997).
[23] D. Besset, B. Favier, L.G. Greeniaus, R. Hess, C. Lechanoine, D. Rapin, and D.W. Werren, Nucl. Instrum. Methods **166**, 515 (1979).
[24] B. A. Brown, A. Etchegoyen, and W. D. M. Rae, computer code OXBASH, MSU version, MSUCL Report No. 524 (1988).
[25] B. Geoffrion, N. Marty, M. Morlet, B. Tatischeff, and A. Willis, Nucl. Phys. **A116**, 209 (1968).
[26] V. Comparat, R. Frascaria, N. Marty, M. Morlet, and A. Willis, Nucl. Phys. **A221**, 403 (1974).
[27] T.W. Donnelly and I. Sick, Rev. Mod. Phys. **56**, 461 (1984).